WELDING RESEARCH

SUPPLEMENT TO THE *WELDING JOURNAL*, 2024
Sponsored by the American Welding Society

Estimation of Bead Size and Catchment Efficiency in Laser Cladding

Cladding procedure variables can be estimated from first principles

BY N. K. KUMAR R., G. WOOD, Y. LU, AND P. F. MENDEZ

Abstract

This paper presents for the first time a set of closed-form predictions for the width, height, and catchment efficiency of laser-clad beads accounting for the distributed nature of the heat source and powder feed. These predictions are based only on known process parameters such as travel speed, laser power, powder feed rate, and material properties. The mathematical analysis is based on the methodology of asymptotics and blending, and the experimental work was performed in actual industrial conditions. To calculate the thermal efficiency of the process, a mathematical expression as a function of powder feed rate is framed, taking into consideration the shadowing due to the powder cloud. In calculating catchment efficiency, the fraction of powders falling on and ahead of the melt pool is calculated and the results reveal that the fraction falling ahead of the melt pool is negligible and does not contribute to the catchment. Predictions are quantitative and within the error expected for industrial conditions and tabulated material properties. Estimates of the height of the bead are greater than the measured height for every case by an average of 18%. Estimates of width and catchment efficiency are within the range of $\pm$ 10%, except for the cases of the low power and higher travel speed domains where a large deviation is observed.

Keywords

- Isotherm Width
- Thermal Efficiency
- Blending
- Powder Cloud

https://doi.org/10.29391/2024.103.016

Introduction

Laser cladding is an overlay deposition technology of applying weld coatings to modify surface characteristics or dimensional build-ups and repair. Using a laser heat source, metallic or composite-based coatings called "clads" are metallurgically bonded to the base material for improved wear or corrosion resistance.

The geometry of the clad bead is a crucial factor in determining necessary information such as the number of overlapping beads required to coat entire surfaces and the number of layer-on-layer passes to target a specific thickness. Of particular interest are practical expressions that practitioners could use without the burden of expertise and time required by numerical models. The trial-and-error approach involving experimental trials to identify the optimal process parameters for the desired dimensions of the clad bead is exhaustive and expensive. These expressions provide an alternative to numerical simulations and experimental trials as an easy-to-implement methodology to make necessary predictions using simple calculation tools with just the input of the process parameters being used.

Analytical models are fast to evaluate and can be accurate when they are formulated properly and calibrated against reliable experiments. Pioneering work on analytical models includes (Ref. 1) for continuous lasers and (Ref. 2). The relationship between catchment efficiency and bead height was also explored in (Ref. 3). Catchment efficiency is the fraction of process powders that become part of the clad bead. Other works involving analytical models of laser cladding include (Refs. 4–7). Experimental work aimed at understanding the factors corresponding to the bead profile include (Refs. 8–10). There are no analytical models to assess catchment, but numerical and experimental work include (Refs. 11–15). In all cases, the assessment of the catchment was numerical or experimental. In (Ref. 16), a model was developed in which bead width was estimated using a Gaussian heat source on a semi-infinite plate (Ref. 17), and catchment efficiency was estimated analytically with some rough simplifications based on a point heat source and the areas of the powder cloud and the weld pool. Recent works (Refs. 18, 19) have used

and expanded on the scaling and blending methodology originally proposed in (Ref. 20).

This work presents a collection of mathematical expressions and an improved methodology for predicting the dimensions of laser-clad beads, accounting for the shadowing due to the powder cloud through an expression for the thermal efficiency of the process. This work introduced an improved analytical estimation of catchment based on proper integration of mass flow over the surface of the weld pool. These estimations are not based on a point heat source but on a Gaussian heat source of the same distribution parameter as the powder flow, which is also assumed to be Gaussian. To check the accuracy of the model, comparisons of the predictions with measured bead dimensions and catchment efficiencies are also provided.

Estimation of Bead Dimensions

Estimation of Bead Width

The mathematical model for predicting the maximum isotherm width (y_{max}) was developed based on the MRC (Minimal Representation and Calibration (Ref. 19) approach. It is based on an idealized conception with a minimal representation of the problem that takes into consideration only the dominant phenomenon involved. Correction factors are then applied to the formula to consider the most important deviations from the ideal case, which can then be calibrated to minimize the deviation between the scaled and exact solutions. Rosenthal's solutions give a minimal representation of the problem (Ref. 21).

One of Rosenthal's solution assumptions is that the laser heat source is a point heat source. Lu (Ref. 18) improved the initial models developed based on the minimal representation by considering the laser heat source to have a Gaussian distribution.

Using a 2-D blending approach, Lu developed an expression for y_{max} which is dependent on only two dimensionless parameters Ry and σ*, where σ is the Gaussian laser power distribution parameter and σ* can be calculated as

$$\sigma^* = \frac{U\sigma}{2\alpha} \tag{1}$$

where U is the target travel speed and α is the thermal diffusivity of the substrate.

The maximum feasible value for σ* is denoted as σ^*_{max}. Above σ^*_{max}, the heat reaching the substrate to the temperature of interest. σ^*_{max} can be calculated using equation (2):

$$\sigma^*_{max} = \left[\left(1.014\ \mathrm{Ry}^{2/3}\right)^n + \left(\sqrt{\frac{\pi}{2}}\mathrm{Ry}\right)^n\right]^{\frac{1}{n}} \tag{2}$$

where $n = -2.644$ (Ref. 22). The maximum isotherm half width applicable for all the regimes in dimensionless form can be calculated using equation (3) (Ref. 18):

$$\widehat{y^*_{max}} = \mathrm{Ry}.\, f_{\mathrm{II-I}}.\, f_{\mathrm{II\text{-}VI}}.\, g \tag{3}$$

where Ry is the Rykalin number, f_{II-I}, f_{II-VI}, and g are correction factors and are defined in detail below.

$$\mathrm{Ry} = \frac{1}{T^*} = \frac{qU}{4\pi k\alpha(T_c - T_0)} \tag{4}$$

In the expression for Rykalin number, q is the effective laser power, U is the target travel speed, T_c is the characteristic temperature, T_0 is the preheat temperature, k is the Thermal conductivity of the substrate, α is the thermal diffusivity of the substrate and T^* is the dimensionless temperature. The effective laser power q is given by equation (5):

$$q = \eta Q \tag{5}$$

where Q is the total power from the heat source. The term f_{II-I} is the correction factor that blends fast and slow-moving concentrated heat source and depends only on Ry. It is given by equation (6),

$$f_{\mathrm{II\text{-}I}} = \left[1 + \left(\sqrt{\frac{2}{e\mathrm{Ry}}}\right)^n\right]^{\frac{1}{n}} \tag{6}$$

where $n = -1.791$ (Ref. 18). The term f_{II-VI} is the correction factor that blends concentrated and distributed slow heat sources and depends only on $\frac{\sigma^*}{\sigma^*_{max}}$. It is given by equation (7),

$$f_{\mathrm{II\text{-}VI}} = \left[\exp\left[a\,.\,n\left(\frac{\sigma^*}{\sigma^*_{max}}\right)^b\right] + \left[\sqrt{2\pi}\left(\frac{\sigma^*}{\sigma^*_{max}}\right)\sqrt{\ln\left(\frac{\sigma^*_{max}}{\sigma^*}\right)}\right]^n\right]^{\frac{1}{n}} \tag{7}$$

where $n = 4.533$, $a = -3.603$, and $b = 13.09$ (Ref. 18). The term g is the correction factor dependent on both Ry and $\frac{\sigma^*}{\sigma^*_{max}}$. It is given by equation (8),

$$g = 1 + \left(0.8170\ \mathrm{Ry}^{\frac{1}{6}} - 1\right)(1 + a_1\mathrm{Ry}^{b_1})^{n_1}\left[1 + a_2\left(\frac{\sigma^*}{\sigma^*_{max}}\right)^{b_2}\right]^{n_2} \tag{8}$$

where $a_1 = 3.859$, $b_1 = -0.5737$, $n_1 = -0.8034$, $a_2 = 0.01703$, $b_2 = -2.202$, and $n_2 = -2.226$ (18).

The engineering expression in dimensional form is given by equation (9) (Ref. 18),

$$y_{\max} = \frac{q}{2\pi k(T_c - T_0)} \cdot f_{\text{II-VI}} \cdot f_{\text{II-I}} \cdot g \tag{9}$$

The width of the clad bead (w) can then be calculated from $y_{\max}$ using the expression,

$$w = 2y_{\max} \tag{10}$$

Estimation of Bead Height

For the estimation of height, the bead is modelled to have a parabolic profile which was shown in (Ref. 21) to be a good approximation. Considering the geometric relation between the area, width, and height of a parabola, the area of the bead (A_b) can be expressed as

$$A_b = \frac{2}{3}wh \tag{11}$$

where w is the width and h is the height of the clad bead. The height of a clad bead can be ascertained by combining three concepts: a mass balance of the process, an understanding of the bead profile of a cross section, and the catchment efficiency of the process. By mass balance, the area of the bead can be presented as a function of powder feed rate ($\dot{m}$), travel speed (U), component powder densities (ρ_c and ρ_m) and catchment efficiency (η_m) of the process. The volume of powders that stay with the bead is the same as the product of area of the bead and the travel speed, thus

$$\frac{\eta_m \dot{m}}{\rho_{\text{eff}}} = A_b U \tag{12}$$

where

$$\rho_{\text{eff}} = f_{vc}\rho_c + (1 - f_{vc})\rho_m \tag{13}$$

Simplification of equation (12) yields the expression for estimation of height of the bead equation as (Ref. 16)

$$h = \frac{3}{2}\frac{\eta_m \dot{m}}{\rho_{\text{eff}} U w} \tag{14}$$

Estimation of Catchment Efficiency

Estimation of catchment efficiency for each bead is based on (Ref. 18). The magnitudes w_l and w_s correspond to the fraction of powders that land on the weld pool and the solid just ahead of the weld bead, respectively. Their expressions are

$$w_l = \left[1 + 0.1322\left(1 - \frac{\sigma_p^*}{\sigma_{p_{\max}}^*}\right)^{-6.155}\right]^{-0.1591} \tag{15}$$

$$w_s = \left[0.9015\left(\frac{\sigma_p^*}{\sigma_{p_{\max}}^*}\right)^{-0.6428} + 0.3040\left(1 - \frac{\sigma_p^*}{\sigma_{p_{\max}}^*}\right)^{-0.3731}\right]^{-2.824} \tag{16}$$

The overall catchment efficiency η_m is given by

$$\eta_m = w_l\eta_l + w_s\eta_s \tag{17}$$

where, η_l is the efficiency of staying (becoming part of the bead) for powders reaching the weld pool, expected to be close to 100% because the powders falling into the liquid are likely to stay there and η_s is the efficiency of staying for powders falling on the solid ahead of the melt pool expected to be close to 0% because the powders falling onto the solid are likely to be blown away by the shielding gas. These efficiencies were determined empirically by minimizing the mean square error between the measured and predicted catchment efficiencies. The measured catchment efficiency is calculated as (Ref. 15):

$$\eta_m = \frac{U}{\dot{m}}\left[A_{b,t} f_{vc}\rho_c + A_{b,r}(1 - f_{vc})\rho_m\right] \tag{18}$$

where, $A_{b,t}$ is the total area of the clad bead, $A_{b,r}$ is the reinforcement area of the clad bead, f_{vc} is the volume fraction of carbide, ρ_c is the density of the carbide powders and ρ_m is the density of the metal powders. The data regarding area, volume fraction, and densities are discussed in the following sections.

Constrained optimization with bounds using the SLSQP algorithm in python was done to minimize the mean square error between the measured and calculated catchment efficiencies, resulting in values of η_l to be 0.7818 and η_s approximately 0.

Experiments

Laser cladding experiments were done to deposit Nickel-Tungsten Carbide composite (Ni-WC) on 4145-MOD Steel.

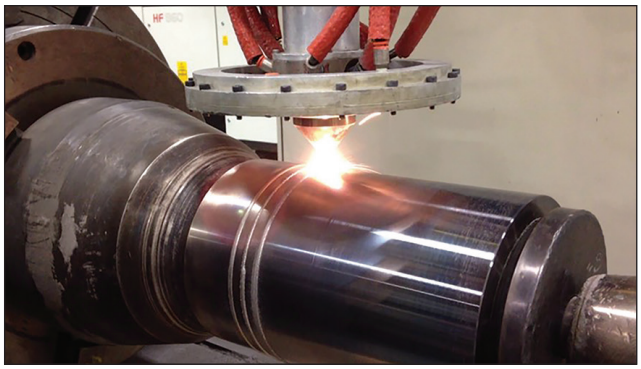

Fig. 1 — Laser Cladding Experiment (Ref. 21).

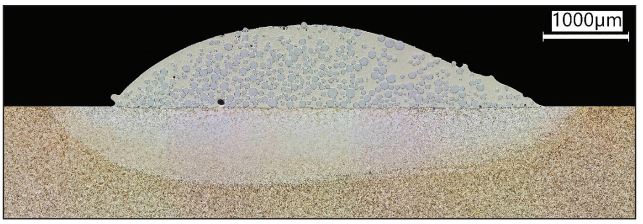

Fig. 2 — Schematic of cross-section of deposited clad bead.

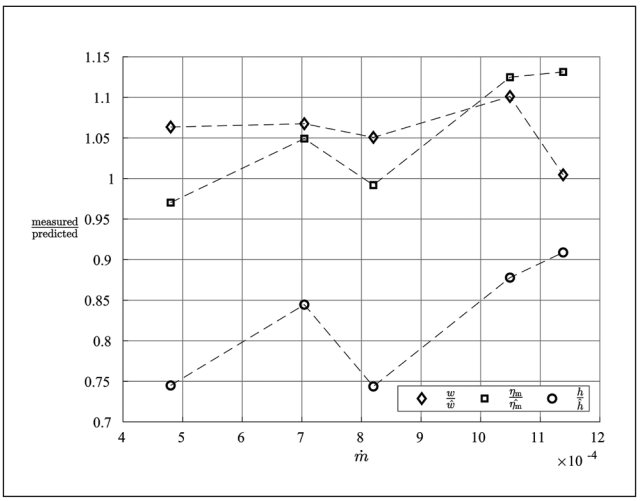

Fig. 3 — Estimation of width, catchment efficiency, and height against powder feed rate at constant laser power and target travel speed.

The power source was a 6 kW CO_2 laser power source with 10.6 microns wavelength. The optics consisted of water-cooled copper-mirror with a final beam focusing mirror focal length of 0.345 m.

Cladding was performed 19 mm beyond the focal point. A disk powder feeder was used to meter powder to the coaxial cladding nozzle capable of powder feed rates up to 0.0055 lb s^{-1} (0.0025 kg s^{-1}) with Ar carrier gas flow at a rate of 0.1680 $in^2\ s^{-1}$ ($1.083 \times 10^{-4}\ m^2\ s^{-1}$). Shielding consisted of argon with a gas flow rate of 21.52 $in^3\ s^{-1}$ ($3.527 \times 10^{-4}\ m^3\ s^{-1}$). The substrate positioning system is a CNC-controlled x-y lathe bed with a mounted four jaw check headstock and tailstock spindle support. Surface rotation speeds were programmed into the CNC system for a given diameter substrate. For the precision equipment used, it was considered that the actual rotation speed matched its set point.

Powder Feed

A mixture of cast spherical fused tungsten carbide and a Ni-Cr-B-Si blend of metal (which comprise the metal matrix in the deposited cladding), is used in this analysis. The carbide chemistry reported by the powder supplier was 3.8 wt-% C and the balance W, which corresponds to a stoichiometry of $WC_{0.6}$. The two component powders were mixed in 60–40% weight fractions of carbide to metal powder, respectively. Properties of the powders such as size range, reported hardness range, weight fractions, and densities are listed in the Table 1.

Experimental Matrix

A total of 13 clad beads were deposited with variations in laser power Q, powder feed rate $\dot{m}$, and travel speed U. The test matrix is set up as a modified fractional factorial design with five levels for each of the three factors. The experimental matrix is presented in Table 2.

Sample Preparation and Analysis

Individual beads were sectioned using a wet saw, mounted, polished to a 0.04 micron finish, and etched for five seconds with 3% Nital to reveal the HAZ. Photomicrographs of sample cross-sections are analysed to measure reinforcement area ($A_{b,r}$), dilution area, total area ($A_{b,t}$) width and height of the bead. $A_{b,r}$ and $A_{b,t}$ are used to calculate the measured catchment efficiency (Ref. 21).

Estimation of Material Properties

The material properties of 4145-MOD Steel substrate are extracted from JMatPro software. Since the width of the clad bead is measured, the characteristic temperature (T_c) to be considered is the melting temperature. The melting temperature is calculated as the average of the solidus (1681.47 K) and liquidus (1758.32 K) temperatures of the 4145-MOD Steel. The value of T_c is calculated as 1720 K. The effective properties are calculated from temperature-dependent properties as indicated in the Appendix.

Estimation of Laser Spot Size and Powder Cloud Diameter

In previous work (Ref. 21), a value of σ (1.620 mm) was obtained by optimization. With the new material parameters and better estimation of catchment, a more accurate value for σ is estimated by minimizing the measured and calculated widths in the 13 experiments performed. In this minimization,

Table 1 — Properties of Powders Used in the Experiments (Ref. 21)

Component	Size Range ($\times 10^{-6}$ m)	Expected Hardness Range in the Deposit (HV)	Weight Fraction (wt-%)	Density (kg m^{-3})
Carbide Powder	45–106	2700–3500	62.60	16,896
Metal Powder	53–150	425.0	37.40	8100

the thermal efficiency was assumed to be affected by the number of powders as discussed in a later section.

Using the Nelder Median Simplex algorithm in python, the optimization is done to minimize the sum of squares of difference between measured and predicted widths, resulting in a value of σ of 1.437 mm, which matches well with the burn marks in acrylic substrate presented in previous work. The value of σ_p is calculated from the powder jet diameter d_p as,

$$\sigma_p = \frac{d_p}{4} \tag{19}$$

The diameter of the powder cloud at its narrowest point was measured in (Ref. 21) as approximately 4 mm to 5 mm. In this work, the value of 5 mm was adopted resulting in an estimated σ_p 1.25 mm.

Estimation of Thermal Efficiency

The experiments suggests that thermal efficiency is affected slightly by the number of powders between the laser optics and the substrate. This effect is captured by the expression,

$$\eta = A - B\dot{m} \tag{20}$$

where, A and B are determined by optimization of the predicted bead width, simultaneously with the laser spot size. On applying Nelder Median Simplex algorithm in python optimization, the values determined are, A = 0.4015 and B = 102.5 kg^{-1} s. The variation of thermal efficiency over the full range of powder flow is between 28% and 35%, with lower values corresponding to the areas experiencing higher shadowing due to increasing powder flow. If Eq. 20 is extrapolated to the case of no powder flow, the value obtained (40.15%) is in close agreement with the published value of the theoretical efficiency of a CO_2 laser with a wavelength of 10.6 micron (40% [Ref. 23]).

Results

The estimated values are compared with the measured values against process parameters, with the estimated values decorated with a ∧ above. The combination of process input parameters is considered as separate test blocks (Target Travel Speed, Laser Power, and Powder Feed Rate). For every test block, five beads with varying values of that parameter are presented and highlighted using dotted lines. These plots give a clear indication of trends when they are present. Good estimations should result in values of the order of 1 on the vertical axis, and no important trends should be observed, as they would indicate both a departure from the target value of 1, and also a systematic error in the predictions.

Prediction on the width of the bead can be done using equation (10). Equation (17) can be used to predict catchment efficiency and requires thermal efficiency calculations developed for the prediction of width. Equation (14) can be used to predict the height of the bead and requires the use of the predicted catchment efficiencies of the bead.

Figure 3 assesses the predictions of bead width, height, and catchment efficiency in the powder feed rate test block. For the range of powder feed rates tested, the width measurements are slightly higher than the estimates without a significant trend. Catchment efficiency does not show any obvious trends against the powder flow.

Figure 4 assesses the predictions of bead width, height, and catchment efficiency in the laser power test block. No discernible trends can be observed for all three predictions beyond scatter. For the lowest laser power, the width measurement is 25% smaller than predicted. Similarly, in the case of catchment efficiency, for the lowest laser power, an over-prediction of approximately 35% is observed.

Figure 5 assesses the predictions of bead width, height, and catchment efficiency in the target travel speed test block. It is not obvious if the apparent trends observed in width and catchment efficiency predictions are meaningful within the scatter. In both cases, over-prediction is observed at the highest speed.

The predictions on width and catchment efficiency in most cases are within a narrow band (±10%) of the measurements. The domains where deviation from the ideal is observed are also consistent in width and catchment efficiency predictions. This overprediction of the width of the bead at high speeds and low beam powers hints at challenges when considering the narrowest beads, as the beam distribution σ approaches σ_{max}.

In all three plots, it can be observed that the height of the bead is overpredicted by 5% to 25%. The height curves show larger departures from the ideal, but no obvious trends can be discerned beyond the scatter.

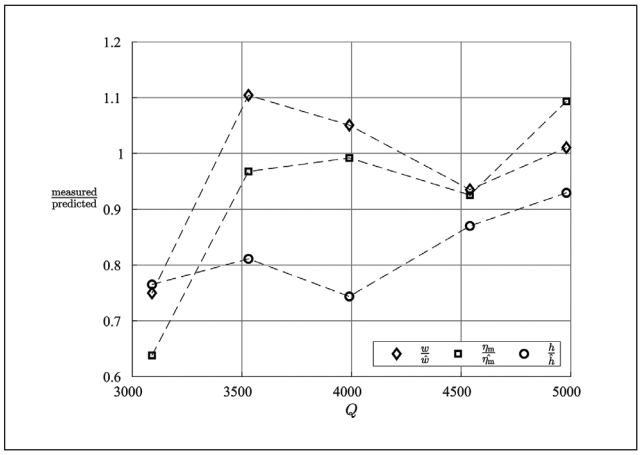

Fig. 4 — Estimation of width, catchment efficiency, and height against laser power at constant powder feed rate and target travel speed.

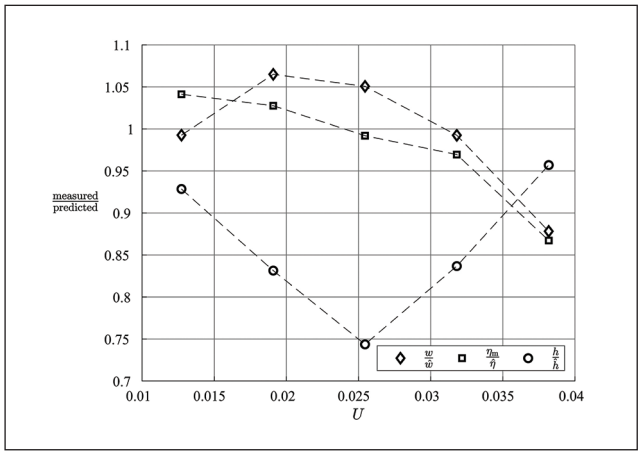

Fig. 5 — Estimation of width, catchment efficiency, and height against target travel speed at constant laser power and powder feed rate.

Table 2 — Experimental Matrix for Cladding of Ni-WC onto a 4145-MOD Substrate for All Beads (Ref. 21)

Bead Number	Laser Power (Q) ($\times 10^3$ W)	Powder Feed Rate ($\dot{m}$) ($\times 10^{-4}$ kg s^{-1})	Target Travel Speed (U) ($\times 10^{-3}$ ms^{-1})	Preheat Temperature (T_0) (K)
Bead 1	4.980	8.200	25.45	530.0
Bead 2	3.090	8.200	25.45	530.0
Bead 3	3.990	8.200	25.45	535.0
Bead 4	3.990	8.200	19.09	531.0
Bead 5	3.990	4.800	25.45	541.0
Bead 6	3.990	8.200	31.81	537.0
Bead 7	4.540	8.200	25.45	536.0
Bead 8	3.530	8.200	25.45	537.0
Bead 9	3.980	8.200	12.73	536.0
Bead 10	3.980	10.49	25.45	537.0
Bead 11	3.980	7.041	25.45	538.0
Bead 12	3.980	8.200	38.18	540.0
Bead 13	3.980	11.38	25.45	537.0

Discussion

The model developed makes predictions of width and catchment within 10% accuracy with the only exception of the highest velocity and the lowest laser power tested. This predictability within a broad range of parameters supports the choice of physics postulated.

At the extremes of low heat input and high travel speed, the extent of molten substrate is at the verge of disappearing, resulting in a normalization against a value that approximates

zero. The system in these conditions is sensitive to variations in parameters and exact profile of the laser beam, and the predictions are extremely sensitive to errors in estimates of parameters and material properties.

The predictions of bead height show a systematic error of 18% in average. A likely source of this error is in the profile of the cross section of the bead, which is not exactly parabolic as assumed here. Hydrostatic pressure flattens the crown of the bead (Refs. 24–26). Small systematic errors as observed here are easy to correct with empirical factors, whether they are constant, or depending on a capillary consideration (e.g., Bond number). Assuming that the cross section of the bead is a portion of a circle as in (Ref. 3) would result in a lower systematic error, but would increase the complexity of the math, still without adding the effect of gravity. The errors obtained are well within of the ±15% repeatability of welding processes assessed in (Ref. 27).

The thermal efficiency was determined empirically as a function of the mass flow, and the value determined for no mass flow (40.15%) is in close agreement with the published value of the theoretical efficiency of a CO_2 laser with a wavelength of 10.6 micron (40% [Ref. 23]). The lower values of thermal efficiency as mass flow increase are consistent with the expected shadowing of the weld pool by the powders.

The catchment efficiency for powders ahead of the weld pool (η_s) was empirically determined as zero, suggesting that none of the powders that fall on the solid metal are incorporated into the bead. The observation during industrial practice is that the shielding gas blows away very quickly all powders that do not enter the weld pool.

The model used uses the same distribution parameter for both the powders and the reasonable beam, given that both distributions are of comparable size in practice. It is possible to account for both separately as in (Ref. 28) at the cost of making the resulting formulas less suited for practical use. In this case, the distribution parameter was considered that of the powders, given that the heat source, even if it is an infinitesimal point, would still result in a weld pool of comparable area. Future experiments will make use of newly acquired beam and powder cloud profilers and should be helpful to reduce uncertainties and empirical calibrations. Although the experimental matrix is only 13 beads with five levels for each variable, it is to be noted that it covers the range of process parameters appropriate in the industrial practice and is sufficient to establish meaningful trends.

Conclusions

A detailed methodology to predict the geometry of the deposited bead has been presented that addresses complexities like thermal efficiency dependence on powder feed rate and material properties dependence on temperatures are discussed. The dimensions of a single laser-clad bead can be estimated accurately with simple calculations and tabulated parameters of great generality. The width of the bead can be estimated using equations (6) to (10). The height of the bead can be estimated using equation (14). The catchment efficiency of the bead can be estimated using equation (17). The thermal efficiency is affected by the deposition of powders and can be estimated using equation (20).

Acknowledgments

This work was supported by MITACS and the Natural Sciences and Engineering Research Council of Canada (NSERC). Valuable discussions and feedback from N. Barnes are gratefully acknowledged.

Nomenclature

y_{max} : Isotherm half width [m]
w : Width of the bead [m]
h : Height of the bead [m]
T : Temperature [K]
T_c : Temperature of Interest [K]
c : Specific heat of the substrate [J kg^{-1} K^{-1}]
k : Thermal Conductivity of the substrate [W m^{-1} K^{-1}]
U : Travel velocity of the moving heat source [m s^{-1}]
q : Effective Laser Power reaching the substrate [W]
Q : Laser Power from the source [W]
$\dot{m}$: Powder feed rate [kg s^{-1}]
α : Thermal diffusivity of the substrate [m^2 s^{-1}]
σ : Gaussian distribution parameter for laser power [m]
σ_p : Gaussian distribution parameter for Powder cloud [m]
ρ : Density of the substrate [kg m^{-3}]
ρ_c : Density of Carbide powders [kg m^{-3}]
ρ_m : Density of Metal powders [kg m^{-3}]
$A_{b,r}$: Reinforcement area of the Bead [m^2]
$A_{b,t}$: Total area of the Bead [m^2]
A_b : Area of the Bead [m^2]
η : Thermal efficiency of the experiment
η_m : Catchment efficiency
η_l : Fraction of powders falling on the melt pool
η_s : Fraction of powders falling in the solid substrate ahead of the melt pool
Ry : Rykalin number
Ro : Rosenthal number
y^*_{max} : Dimensionless Isotherm half width
I : Regime I (Large Ry, small σ*, fast point heat source)
II : Regime II (Small Ry, small σ*, slow point heat source)
V : Regime V (Large Ry, large σ*, fast distributed heat source)
VI : Regime VI (Small Ry, large σ*, slow distributed heat source)

References

1. Lemoine, F., Grevey, D., and Vannes, A. 1993. Cross-section modeling laser cladding. *Proceedings of SPIE - The International Society for Optical Engineering*: 203–212.

2. Lemoine, F., Grevey, D., and Vannes, A. 1994. Cross-section modeling of pulsed Nd:YAG laser cladding. *Proceedings of SPIE - The International Society for Optical Engineering*: 37–44.

3. Colaço, R., Costa, L., Guerra, R., and Vilar, R. 1996. A simple correlation between the geometry of laser cladding tracks and the process parameters. in laser processing: Surface treatment and film deposition. *Kluwer Academic Publishers*: 421–429.

4. Pinkerton, A. J., and Lin, L. 2004. Modelling the geometry of a moving laser melt pool and deposition track via energy and mass balances. *Journal of Physics D: Applied Physics* 27: 1885–1895.

5. Lalas, C., Tsirbas, K., Salonitis, K., and Chryssolouris, G. 2007. An analytical model of the laser clad geometry. *International Journal of Advanced Manufacturing Technology*: 32: 34–41.

6. El Cheikh, H., Cournat, B., Hascoët, Jy., and Guillén, R. 2012. Prediction and analytical description of the single laser track geometry in direct laser fabrication from process parameters and energy balance reasoning. *Journal of Materials Processing Technology* 212: 1832–1839.

7. Peyre, P., Aubry, P., Fabbro, R., Neveu, R., and Longuet, A. 2008. Analytical and numerical modelling of the direct metal deposition laser process. *Journal of Applied Physics D: Applied Physics* 41(2): 1–10.

8. Oliveira, U., Ocelík. V., De Hosson, J. T. M. 2005. Analysis of coaxial laser cladding processing conditions. *Surface and Coatings Technology* 197: 127–136.

9. Davim, J. P., Oliveira, C., and Cardoso, A. 2008. Predicting the geometric form of clad in laser cladding by powder using multiple regression analysis (MRA). *Materials & Design* 29: 554–557.

10. Nenadl, O., Ocelík, V., Palavra A, and De Hosson, J. T. M. 2014. The prediction of coating geometry from main processing parameter in laser cladding. *Physics Procedia* 56: 220–227.

11. Picasso, M., Marsden, C. F., Wagniére, J. D., Frenk, A., and Rappaz, M. 1994. A simple but realistic model for laser cladding. *Metallurgical and Materials Transactions B* 25(2): 281–291.

12. Lin, J., and Steen, W. M. 1997. Powder flow and catchment during coaxial laser cladding. *In Lasers in Materials Processing: The International Society for Optical Engineering* 517–524.

13. Frenk, A., Vandyoussefi, M., Wagniére, J. D., Zryd, A., and Kurz, W. 1997. Analysis of the laser cladding process for stellite on steel. *Metallurgical and Materials Transactions B* 25(3): 501–508.

14. Partes, K. 2009. Analytical model of the catchment efficiency in high speed laser cladding. *Surface and Coatings Technology* 204: 366–371.

15. Wood, G., and Mendez, P. F. 2015. Disaggregated metal and carbide catchment efficiencies in laser cladding of nickel-tungsten carbide. *Welding Journal* 94(11): 343-s to 350-s.

16. Wood, G., and Mendez, P. F. 2016. First order prediction of bead width and height in coaxial laser cladding. *Institute of Materials Science, Joining and Forming*.

17. Eagar, T. W., and Tsai, N. S. 1983. Temperature Fields Produced by Traveling Distributed Heat Sources. *Welding Journal*: 346-s to 355-s.

18. Yi, L. 2021. A systematic methodology to develop scaling laws for thermal features of temperature field induced by a moving heat source. PhD Thesis. Alberta: University of Alberta.

19. Mendez, P. F. 2020. Reduced Order Models for Welding and Solidification Processes. *IOP Conference Series Materials Science and Engineering* 861(1): 01200.

20. Churchill, S. W., and Usagi, R. 1974. A standardized procedure for the production of correlations in the form of a common empirical equation. *Industrial & Engineering Chemistry Fundamentals* 13(1): 39–44.

21. Wood, G. 2017. Heat and mass transfer aspects of coaxial laser cladding and it's application to nickel-tungsten carbide alloys. PhD Thesis. Alberta: University of Alberta.

22. Wang, Y. 2021. Design rules for characteristics of heat flow in welding on thick plates using asymptotics and blending. PhD Thesis. Alberta: University of Alberta.

23. Duley, W. W. 1976. *CO_2 Lasers: effects and applications*. Academic Press.

24. Matsunawa, A. 1984. Role of surface tension in fusion welding (part 3). *Transactions of JWRI* 13(1): 147–156.

25. Matsunawa, A, and Ohji, T. 1983. Role of surface tension in fusion welding (part 2): Hydrostatic effect. *Transactions of JWRI* 12(1): 123–130.

26. Matsunawa A, Ohji T. 1982. Role of surface tension in fusion welding (part 1). *Transactions of JWRI* 11(2): 145–154.

27. Duman, U. 2009. Modeling of weld penetration in high productivity GTAW. PhD Thesis. Golden, Colorado: Colorado School of Mines, Metallurgical and Materials Engineering.

28. Grams, M. R. 2023. Optimization of powder catchment efficiency for industrial laser. *16th International Conference on Modelling of Casting, Welding and Advanced Solidification Processes* 1281: 012006.

Appendix

Effective Thermal Conductivity

The best way to obtain an effective thermal conductivity k_{eff} is to consider the overall thermal resistance of a wall of thickness d in steady state.

$$R'' = \frac{\Delta T}{q''} = \frac{d}{k_{\text{eff}}} \tag{21}$$

where R'' is the thermal resistance associated with the absolute values of heat flux q'' and temperature difference ΔT through the thickness d of the wall. Fourier's law indicates

$$q'' = -k(T)\frac{dT}{d\xi} = constant \tag{22}$$

where $T = T(\xi)$, ξ is the 1-D spatial coordinate and $k = k(T)$. The constant value of this equation is because it is in steady state, so there can be no accumulation or depletion of heat at any point in the wall. The temperature difference between the surfaces of the wall can be calculated by integration of the equation. The result of integration and the equation together gives

$$k_{\text{eff}} = \frac{1}{\Delta T}\int_0^L k(T)\,dT \tag{23}$$

In summary, the best practical choice for effective thermal conductivity is to consider the average of thermal conductivity over the temperature range of interest. Equation (23) is thus used for calculations in this work. For the case of melting, the suggested range of temperature is between T_0 and T_{melt} (the mean of T_{solidus} and T_{liquidus}).

Effective Specific Heat

To calculate the effective value of specific heat, averaging the value of c is potentially problematic since, phase changes can be missed or underestimated in the resolution of thermodynamic calculations. A better approach is to start with the definition of specific heat,

$$c = \frac{di}{dT} \tag{24}$$

from which an effective volumetric specific heat *pc* can be approximated as

$$(\rho c)_{\text{eff}} \approx \frac{\Delta \rho i}{\Delta T} \tag{25}$$

where ΔT is the range of temperature of interest, typically between T_0 and T_m.

Effective Thermal Diffusivity

Based on the effective values of volumetric specific heat $(pc)_{\text{eff}}$ and the thermal conductivity (k_{eff}), the effective thermal diffusivity (α_{eff}) can be calculated using the relationship

$$\alpha_{\text{eff}} = \frac{k_{\text{eff}}}{(\rho c)_{\text{eff}}} \tag{26}$$

Effective Thermophysical Properties for all Beads

Table 3 — Effective Thermophysical Properties

Bead Number	k_{eff} ($Wm^{-1}K^{-1}$)	α_{eff} ($\times 10\text{-}6 m^2 s^{-1}$)	ρ_{eff} ($\times 10^3$ kg m^{-3})	c_{peff} ($Jkg^{-1}K^{-1}$)
Bead 1	33.10	5.593	7.555	783.3
Bead 2	33.10	5.593	7.555	783.3
Bead 3	33.04	5.577	7.554	784.2
Bead 4	33.08	5.590	7.554	783.5
Bead 5	32.96	5.557	7.553	785.3
Bead 6	33.01	5.570	7.553	784.6
Bead 7	33.02	5.573	7.554	784.4
Bead 8	33.01	5.570	7.553	784.6
Bead 9	33.02	5.573	7.554	784.4
Bead 10	33.01	5.570	7.553	784.6
Bead 11	33.00	5.567	7.553	784.7
Bead 12	32.97	5.560	7.553	785.1
Bead 13	33.01	5.570	7.553	784.6

NITHEESH KUMAR RAMASAMY is with the National Institute of Technology, Tiruchirappalli, Tiruchirappalli, Tamil Nadu, India. **GENTRY WOOD** is with Apollo-Clad Laser Cladding. Lastly, **LU YI** and **PATRICIO F. MENDEZ** (*pmendez@ualberta.ca*) are with the University of Alberta**.**